Icarus 221 (2012) 310–319

Contents lists available at SciVerse ScienceDirect

Icarus

journal homepage: www.elsevier.com/locate/icarus

Low-velocity collisions between centimeter-sized snowballs: Porosity dependence of coefficient of restitution for ice aggregates analogues in the Solar System

Yuri Shimaki [a,*], Masahiko Arakawa [b,1]

[a] Graduate School of Environmental Studies, Nagoya University, Furo-cho, Chikusa-ku, Nagoya 464-8601, Japan
[b] Graduate School of Science, Kobe University, 1-1 Rokkodai-cho, Nada-ku, Kobe 657-8501, Japan

ARTICLE INFO

Article history:
Received 13 April 2012
Revised 4 July 2012
Accepted 3 August 2012
Available online 17 August 2012

Keywords:
Ices, Mechanical properties
Collisional physics
Planetary formation
Planetary rings
Comets

ABSTRACT

Understanding the collisional behavior of ice dust aggregates at low velocity is a key to determining the formation process of small icy bodies such as icy planetesimals, comets and icy satellites, and this collisional behavior is also closely related to the energy dissipation mechanism in Saturn's rings. We performed head-on collision experiments in air by means of free-falling centimeter-sized sintered snowballs with porosities from 44% to 80% at impact velocities from 0.44 m s^{-1} to 4.12 m s^{-1} at −10 °C. In cases of porosity larger than 70%, impact sticking was the dominant collision outcome, while bouncing was dominant at lower porosity. Coefficients of restitution of snow in this velocity range were found to depend strongly on the porosity rather than the impact velocity and to decrease with the increase of the porosity. We successfully measured the compaction volume of snowballs after the impact, and it enabled us to estimate the dynamic compressive strength of snow with the assumption of the energy conservation between kinetic energy and work for deformation, which was found to be consistent with the upper limit of static compressive strength. The velocity dependence of coefficients of restitution of snow was analyzed using a Johnson's model, and a diagram for collision outcomes among equal-sized sintered snowballs was successfully drawn as a function of porosity and impact velocity.

1. Introduction

It is widely accepted that proto-planets were formed in the proto-planetary disk (PPD) through mutual collisions and accretion of planetesimals, which were kilometer-sized bodies with sufficient gravitational attraction force and would be made of dust aggregates growing in the PPD. The origin of planetesimals has been studied by many authors, but it remains an unresolved problem that is still under debate. Thus, there are two main hypotheses about the origin of planetesimals: they are a "gravitational instability model" of a dense dust layer in the solar nebula (e.g., Goldreich and Ward, 1973) and a "dust coagulation model" of adhesion force occurring among dusts and aggregates (e.g., Weidenschilling and Cuzzi, 1993). However, in both cases the collision among dust aggregates would have taken place during the early growth process of planetesimals, and the efficiency of the impact sticking could be affected by the physical properties of the dust aggregates and would control the subsequent growth process.

The dust aggregates in the PPD grew through mutual collisions among initially micron-sized dust grains. The tiny dust grains in a gas disk naturally collided with each other in Brownian motion and stuck together at collision velocities under 10^{-3} m s^{-1} to result in fractal dust aggregates (Blum et al., 2000; Blum, 2010). At the next stage of the nebula process, the aggregates grew depending on their sizes through mutual collisions due to vertical settling into mid-plane, differential drift motion and gas turbulence in the solar nebula (Weidenschilling and Cuzzi, 1993). However, as the aggregates grew, their radial drift due to gas drag caused material depletion through the physical process of falling into the central star, and the radial drift of the aggregates also caused the increase of the relative collision velocity among dust aggregates up to 50 m s^{-1}. Such a large collision velocity would initiate fragmentation of the aggregates, and therefore it was not clear how planetesimals could form only through the coagulation of dust aggregates (e.g., Weidenschilling, 1977).

The coagulation process of silicate dust aggregates in the PPD has been studied by both numerical simulations and laboratory experiments in past decades (e.g., Blum, 2010). Güttler et al. (2010) reviewed various collision experiments among silicate dust aggregates and nonporous materials, and they classified the collision outcomes into several types, such as sticking, bounce

* Corresponding author. Fax: +81 78 803 6684.
E-mail address: shimaki@eps.nagoya-u.ac.jp (Y. Shimaki).
[1] Fax: +81 78 803 6684.

0019-1035/$ - see front matter © 2012 Elsevier Inc. All rights reserved.
http://dx.doi.org/10.1016/j.icarus.2012.08.005

and fragmentation. They found that several key parameters would determine these collision outcomes for silicate dust aggregates: the collision velocity, the size ratio of two colliding bodies and mass of the smaller body, and the porosity, ϕ, of colliding dust aggregates. The parameter ϕ is also described by a volume filling factor ($f = 1 - \phi$) with a physical meaning such as a volume fraction filled with material. According to the compiled data of Güttler et al. equal-sized porous silicate dust aggregates were disrupted at collision velocities higher than 1 m s^{-1}, and the sticking velocity decreased with the increase of aggregate masses. Using this compiled data, Zsom et al. (2010) conducted a numerical simulation of the collision evolution of silicate dust aggregates in the PPD, and they found that the growth of dust aggregates halted at masses of ~0.1 g in the minimum mass solar nebula model because of bouncing among compacted dust aggregates, so that the largest aggregates only reached the centimeter size. Thus, the silicate dust aggregates in their numerical model could not grow over this threshold size of ~cm due to the so-called 'bouncing barrier'.

To reveal the collision behavior of centimeter-sized dust aggregates in micro-gravity condition, Beitz et al. (2011) performed collision experiments of centimeter-sized SiO_2 dust spheres with $f = 0.49$–0.54 at the collision velocity of 0.01–2 m s^{-1}. They found that at velocities lower than 0.2 m s^{-1} the collision outcome was bouncing, but velocities higher than 0.2 m s^{-1} resulted in fragmentation of one dust sphere with little mass transfer to another one or catastrophic disruption of both. The coefficient of restitution, ε, of the dust sphere in the bouncing collision was found to scatter without correlation to the impact velocity or the impact parameter (b/D), which is defined as the perpendicular distance, b, between the path of a projectile and the geometrical center of the target normalized by the sample diameter, D, which was determined to be $\varepsilon = 0.35 \pm 0.12$. However, the coefficient of restitution is widely accepted to change with several factors, such as impact velocity, bulk porosity, surface roughness and physical properties such as yield strength. The coefficient of restitution of silicate dust aggregates was already found to decrease with the increase of porosity (Beitz et al., 2011).

Fujii and Nakamura (2009) performed low-velocity impact experiments between a steel plate and a gypsum sphere with the porosity ranging from 0% to 61% and the diameter from 25 mm to 83 mm at velocities up to 20 m s^{-1}. They measured the coefficient of restitution and the collision deformation of the gypsum and found that the coefficient of restitution of a gypsum sphere decreased from 0.7 to 0.1 with the increase of the impact velocity for gypsum with the diameter of 50 mm. They did not find a clear dependence of the coefficient of restitution on the porosity up to $\phi = 61\%$.

In contrast to the 'bouncing barrier' of silicate dusts, ice dust aggregates might overcome this kind of a special barrier that prohibits coagulation. According to a series of numerical simulations for ice aggregate collisions based on a particle interaction model (Suyama et al., 2008; Wada et al., 2007, 2008, 2009), fractal dust aggregates with the porosity larger than 99% composed of submicron ice dust particles could stick together at velocities up to 10 m s^{-1} with little compaction. They found that the maximum collision velocity necessary for the net growth of ice dust aggregates is about 50 m s^{-1}, but that of silicate dust aggregates is about 5 m s^{-1}, which is one order of magnitude smaller than that of ice aggregates, due to the difference of their surface energies (Wada et al., 2009). Additionally, Wada et al. (2011) studied the effect of filling factor on sticking condition and showed that collisional sticking of ice and silicate aggregates occurred when their mean filling factors are less than ~0.3, irrespective of their materials or structures.

Dust aggregates were compacted during the collision when the impact energy was high enough to restructure particle chains connected with each other by a van der Waals force (Suyama et al., 2008). Okuzumi et al. (2009) developed a numerical model for mass and porosity evolution of silicate dust aggregates in the PPD and found that the maximum density of dust aggregates was still quite small (10^{-4} g cm^{-3}). Repeated dynamic compaction of silicate dust aggregates was also studied by laboratory experiments. Weidling et al. (2009) conducted repeat-bouncing experiments of silicate dust aggregates with $f = 0.15$ on a solid plate at 0.2 m s^{-1} and studied the porosity evolution caused by the bouncing with the repeat number. They found that after about 2000 collisions the filling factor almost reached the equilibrium value, $f = 0.36$. This result indicates that the porosity of aggregates could decrease with the number of bouncing or collision incidents. Thus, the porosity of ice dust aggregates would also change with the aggregates' collision history and affect the collision outcomes. In addition to the porosity, sintering among ice particles of aggregates might be important around a snow line in the solar nebula, as it would enhance the rigidity of aggregates and result in collisional bounce (Sirono, 1999).

Research has shown that low-velocity collisions among ice particles have played an important role in the evolution of planetary ring systems. Saturn's dense ring system consists of a large number of water ice particles ranging in size from 1 cm to 10 m, and they orbit in Keplerian motion with a relative velocity on the order of cm s^{-1} (Cuzzi et al., 2009; Schmidt et al., 2009). The collisions among ice particles in planetary rings could determine the steady state structure of the ring, such as ring thickness and ring lifetime and thus the coefficients of restitution of ice spheres were measured for water ice to estimate the energy dissipation rate during collisions among ring particles with thin frost (Bridges et al., 1984) and without frost (Hatzes et al., 1988; Higa et al., 1996, 1998). Bridges et al. (1984) showed that the coefficient of restitution of water ice was reduced even by a thin frost layer, which indicated that the surface properties, namely the porosity, strongly affected energy dissipation during collision.

In this study, we performed low-velocity impact experiments of centimeter-sized sintered snowballs with porosity ranging from 44% to 80%. We also studied the porosity dependence of sticking velocities between equal-sized snowballs and the coefficient of restitution of snowballs in bouncing. Then, we examined the porosity dependence of the dynamic compressive strength of snow and estimated the impact conditions for collision sticking. Section 2 describes the sample preparation and the experimental procedures, and Section 3 gives the experimental results on the coefficient of restitution and on the contact area during each collision. Section 4 discusses the physical mechanisms of collision deformation and sticking.

2. Experimental methods

2.1. Sample preparation

Spherical snow samples with different porosities were prepared by using small ice particles in a cold room at -10 ± 0.5 °C at the Institute of Low Temperature Science, Hokkaido University. The ice particles used to make the samples had an average diameter of 21 ± 15 μm, where the error denotes a standard deviation, and were prepared by freezing small water droplets splashed from a special nozzle in liquid nitrogen. The frozen droplets were preserved in liquid nitrogen to prevent them from sintering and sublimation. The ice particles were brought out of liquid nitrogen just before making the spherical samples and dried in a cold room.

The ice particles were put into a spherical stainless steel mold with a diameter of 30 mm and sieved through a 1.5-mm opening mesh to attain large initial porosity. Thus, the sample was

Table 1
Experimental conditions and results.

Run number	Average porosity	m_t (g)	m_p (g)	v_i (m s^{-1})	b/D (–)	ε (–)	W (mm)	Sintering duration	Collisional type
Porosity = 44%									
110928-13	0.443	7.44	7.49	0.44	0.069	0.250 ± 0.023	1.95 ± 0.07	2 days	Bounce
110928-2	0.441	7.57	7.45	1.54	0.122	0.130 ± 0.009	4.70 ± 1.01	2 days	Bounce
110927-2	0.438	7.52	7.52	3.50	0.035	0.186 ± 0.003	5.58 ± 2.38	2 days	Bounce
Porosity = 52%									
110928-14	0.522	6.20	6.47	0.57	0.069	0.105 ± 0.020	2.75 ± 0.21	2 days	Bounce
110928-1	0.520	6.34	6.33	1.45	0.000	0.041 ± 0.017	4.85 ± 0.21	2 days	Bounce
110927-8	0.528	6.10	6.27	3.57	0.072	0.087 ± 0.002	9.10 ± 2.27	1 day	Bounce
Porosity = 60%									
110928-9	0.602	5.21	5.14	0.70	0.029	0	5.15 ± 0.07	2 days	Sticking
110928-3	0.605	5.18	5.07	1.61	0.043	0.031 ± 0.011	7.93 ± 1.50	2 days	Bounce
110927-3	0.607	5.10	5.08	3.36	0.046	0.029 ± 0.001	9.53 ± 1.30	1 day	Bounce
Porosity = 70%									
110928-10	0.691	3.83	3.84	0.79	0.110	0	8.73 ± 3.80	1 day	Sticking
110928-11	0.702	3.88	3.84	0.85	0.105	0	6.60 ± 0.57	15 min	No-bounce
110928-6	0.701	3.88	3.88	1.63	0.070	0	8.75 ± 1.06	15 min	Sticking
110928-4	0.695	3.86	3.78	1.95	0.000	0	12.8 ± 2.8	2 days	Sticking
110927-7	0.707	3.73	3.86	3.17	0.000	0	13.3 ± 0.3	15 min	Sticking
110927-4	0.696	3.85	3.86	3.48	0.101	0	13.9 ± 4.2	1 day	Sticking
110929-2	0.703	3.88	3.81	4.12	0.074	0	13.8 ± 0.8	15 min	Sticking
Porosity = 80%									
110928-12	0.800	2.61	2.58	0.85	0.113	0	7.6 ± 1.0	15 min	No-bounce
110928-5	0.799	2.59	2.62	1.73	0.060	0	13.4 ± 0.2	15 min	Sticking
110929-3	0.799	2.61	2.61	2.03	0.017	0.030 ± 0.002	16.3 ± 2.2	15 min	Bounce
110927-6	0.800	2.60	2.58	3.39	0.093	0	15.3 ± 0.1	15 min	Sticking

constructed by agglomerated ice particles with the maximum size of sub-mm: the initial internal structure would have pores with the size less than sub-mm. To control the sample porosity from 44% to 80%, we changed the mass of the ice particles put into one concaved hemispherical mold from 7.57 to 2.54 g. Ice particles in this mold were compressed gently by hand against another concaved hemispherical mold to form a spherical sample, which had a homogeneous interior and a smooth spherical surface. After the compression, the sample was taken out of the mold and preserved in a sealed plastic bag at a temperature of −10 °C and was sintered for a period from 15 min to 2 days, which allowed us to check the effect of sintering duration on the sample strength. An average particle size was 40 ± 17 μm for the sample sintered for 15 min and 74 ± 25 μm for the sample sintered for 1 day. We did not use 80% porosity samples sintered for more than 1 day, because they were deformed into ellipsoidal shape due to their own weight during sintering. A small amount of red ink was added to the water to color ice particles, and we made a colored snowball as the target. This colored target allowed us to distinguish the projectile fragments from the target fragments. We confirmed that the addition of red ink did not affect the physical properties of the snowball related to the impact phenomena significantly by conducting an impact test using a snowball with and without red ink. All experimental conditions and results are shown in Table 1.

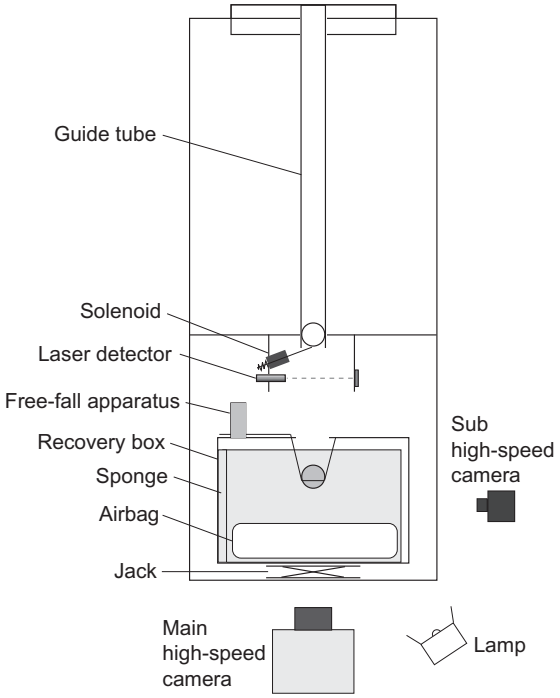

Fig. 1. Schematic illustration of the experimental setup.

2.2. Experimental setup

Low-velocity collision experiments were carried out in air by a free-fall apparatus using a two-level release mechanism installed in the cold room at −10 ± 0.5 °C, and it enabled two porous snowballs with the same porosity to collide at impact velocities between 0.44 and 4.12 m s^{-1} (Fig. 1). For impact velocities lower than 1.4 m s^{-1}, the projectile sample was set at the bottom of a guide tube and supported by a solenoid needle before the experiment. The solenoid released the projectile by a spring attached on the needle to allow the projectile to drop in free fall. For impact velocities greater than 1.4 m s^{-1}, the projectile was dropped from the top of the guide tube. The target sample was suspended by nylon threads in a transparent recovery box with a height of 25 cm to recover the collided samples. To avoid secondary collision of samples on the bottom and sidewalls, a plastic airbag was set on the bottom of the box, and two sides of the box were covered by sponge plates, although the other two sides were uncovered to observe collisional behavior by high-speed cameras. A laser beam and photodiode were installed between the guide tube and the recovery box, and they were used as the trigger to initiate the free-fall apparatus. When a projectile cut off the laser beam, the solenoid was switched on to release the threads and the target dropped in free fall. The

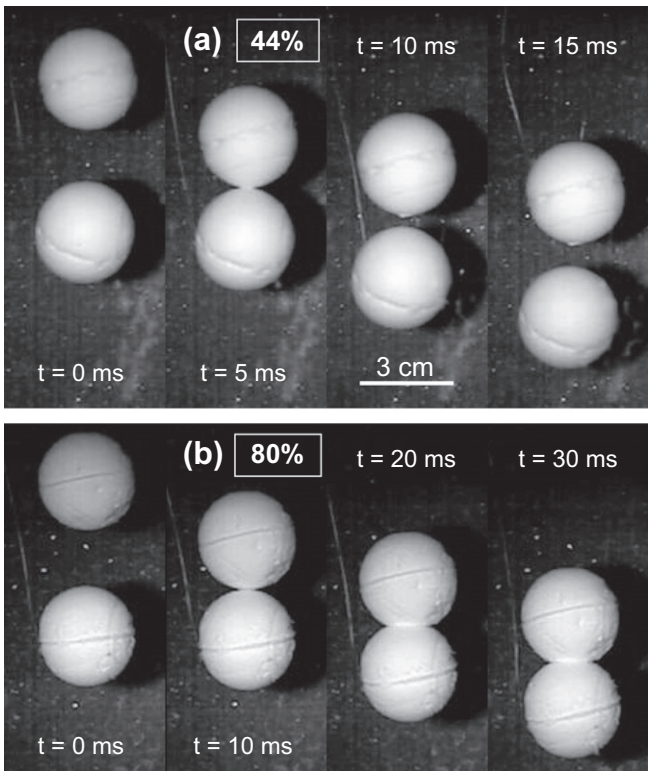

Fig. 2. Image sequences of typical collisions. (a) Bouncing collision between 44% porosity snowballs at $v_i = 3.5\ \mathrm{m\ s^{-1}}$. Small fraction of mass transferred to the projectile at its bottom. (b) Sticking collision between 80% porosity snowballs at $v_i = 1.7\ \mathrm{m\ s^{-1}}$. Time after the impact is shown in the figure. The bright line in the figure was a thin nylon thread. Run numbers are (a) 110927-2 and (b) 110928-5.

projectile usually collided with the free-falling target in a head-on impact (Fig. 2). The relative impact velocity was mainly controlled by the initial distance between the projectile and the target.

The collision behavior was recorded by two high-speed video cameras mounted mutually perpendicular to the impact direction in order to measure the impact velocity and the impact angle between the two snowballs. The main high-speed camera (NAC MEMRECAM fx-K3) was set in front of the box and had a shutter speed of 0.1 or 0.05 ms, a frame rate of 1000 or 2000 frames per second and an image size of 640 × 480 pixels. The typical spatial resolution was 0.4 mm/pixel. The main cameras observed more than 50 frames during the impact. Thus, the lowest velocity that we could measure in our system was 0.4 (mm)/50 (ms) = 0.008 (m s^{-1}), and the lower limit of the coefficient of restitution that we could determine was from 0.0019 to 0.018, depending on the impact velocity. The sub high-speed camera (CASIO EX-F1) was set at the side of the box and had a shutter speed of 0.1 ms, a frame rate of 300 frames per second and an image size of 512 × 384 pixels. The typical spatial resolution was 0.54 mm/pixel for the sub camera. A metal halide lamp was used to illuminate the target.

The relative impact and rebound velocities during collision were analyzed using high-speed video images. We attempted to perform a head-on collision between snowballs. The impact parameter, b, was calculated to be $b^2 = b_1^2 + b_2^2$, where b_1 and b_2 were two-dimensional (2-D) impact parameters determined from each camera direction, respectively. The impact parameter normalized by the sample diameter (b/D) was regulated to be less than 0.12.

Additionally, three collision experiments among sintered snow samples with the same porosities but different masses were carried out. The projectile was a sphere with a diameter of 10 mm, and the target was a cylinder with a height and a diameter of 100 mm. Both samples were prepared in the same way as described above at a room temperature of −15 °C. The porosity of the samples was 40%, 50% and 60%. The projectiles were accelerated by free-fall and collided with the flat surface of the target, and the rebounded motion was recorded by a high-speed camera.

3. Results

3.1. Coefficient of restitution

All of the collisional outcomes were classified into bounce, no-bounce or sticking according to the analysis of recorded video images. Fig. 2a shows typical bouncing collision for 44% porosity samples impacted at the velocity of 3.5 m s^{-1}. Mass transfer from the target to the projectile was recognized in the recorded image (details are discussed in Section 3.2). Fig. 2b shows typical sticking collision between 80% porosity samples impacted at the velocity of 1.7 m s^{-1}. Two porous snowballs stuck together after the collision and dropped in translational motion as a dimer. However, they usually separated after landing on an airbag because the sticking force between them was not large enough to withstand the impact force on the airbag, although we recovered an adhered dimer on the airbag in one experiment (Fig. 4c). No-bounce collision, which is defined as the collision with the departing velocity between snowballs less than 0.02 m s^{-1}, which corresponded to $\varepsilon < \sim 0.025$, but without adhesion between them, was observed for the 70% and 80% porosity samples. The no-bounce mode sometimes appeared when the struck snowballs were separated by the tensional force of threads that were insufficiently released from the free-fall apparatus.

The relative impact and rebound velocity (v_i, v_r) were analyzed from high-speed video images just before and after collision. Since all collisions were nearly head-on with $b/D < 0.12$, the coefficient of restitution of the snowball sample was defined as the ratio of v_r to v_i in the normal direction, as follows:

$$\varepsilon = v_r / v_i. \tag{1}$$

The energy dissipation rate during bouncing collision can be represented by $1 - \varepsilon^2$. Fig. 3 shows the relationship between the coefficient of restitution and (a) the impact parameter, (b) the impact velocity and (c) the filling factor of the samples. We found that the coefficient of restitution of snow was almost independent of the impact parameter up to $b/D = 0.12$ (Fig. 3a). The dependence of the coefficient of restitution on the impact velocity was unclear (Fig. 3b). For the 44% and 52% porosity samples, the coefficient of restitution became the minimum at $v_i = 1.6\ \mathrm{m\ s^{-1}}$, but for the 60% porosity it reached 0 even at the smallest impact velocity of 0.7 m s^{-1} and for porosities larger than 70% it was almost 0 in this velocity range, except for one 80% result. In this exception the projectile rotated slightly before the collision.

Coefficients of restitution for porous material were reported to be scattered, which was caused by surface roughness (e.g., Beitz et al., 2011; Fujii and Nakamura, 2009; Heiβelmann et al., 2010). However, we found that the coefficient of restitution of snow clearly decreased with the decrease of the filling factor and was nearly 0 at $f = 0.3$ (Fig. 3c). In addition to the equal-sized collision, we changed the size ratio of the impacting snowball to the target. A 10-mm snowball was impacted on a flat surface of a large cylinder target with the size of 100 mm at $v_i = 2$–$3\ \mathrm{m\ s^{-1}}$, and we found that the results were comparable to those obtained for the equal-sized collisions. This means that the coefficient of restitution does not depend on the size ratio so much, or that the scattering of the measured coefficient of restitution was too large to recognize the dependence of the size ratio.

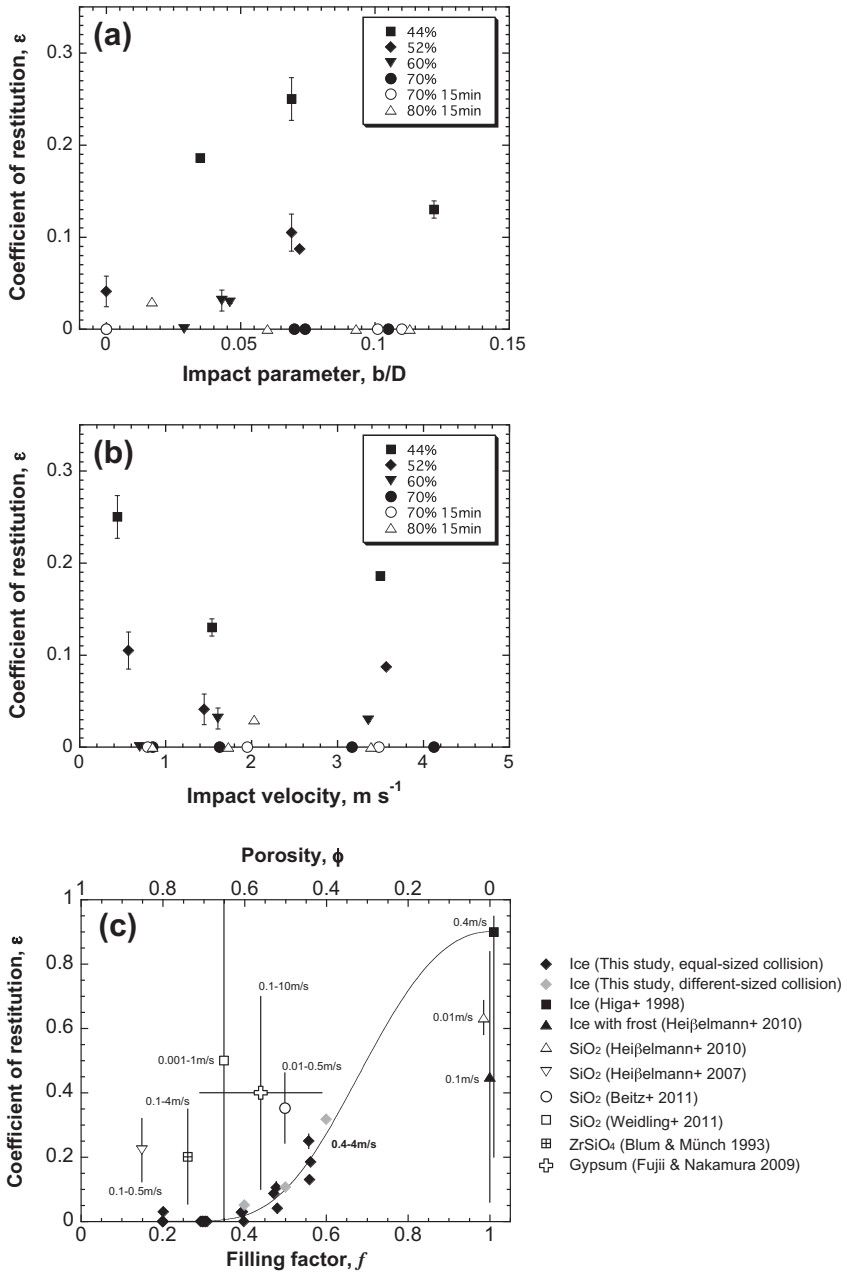

Fig. 3. The relationships between the coefficient of restitution of snow and (a) the impact parameter, (b) the impact velocity, and (c) the filling factor. (a and b) Filled symbols indicate a sintering duration of 1 or 2 days, and open symbols indicate a sintering duration of 15 min. (c) The referenced data are summarized in Table 2. The solid curve is the empirical result of Eq. (2).

The coefficients of restitution for a crystalline ice ball with the diameter of 30 mm was measured by Higa et al. (1996), and it was obtained for collisions on a large ice block. The result at $v_i = 0.4$ m s^{-1} and -10 °C is shown in Fig. 3c. They found the coefficient of restitution of ice decreased with the increase of velocity between 0.35 and 5 m s^{-1}, though the data were scattered and had large errors. The coefficient of restitution for crystalline ice was also obtained by the collisions among ice balls with the diameter of 15 mm at $v_i = 0.06$–0.22 m s^{-1}, as plotted in Fig. 3c, but the ice surface was covered by frost (Heiβelmann et al., 2010). The frost consisted of tiny ice grains that could cause an increase of local porosity at the impact point, which would reduce the coefficient of restitution. Thus, the coefficient of restitution on a non-frosted ice surface should be chosen to be about 0.9. Using our results and those of Higa et al. (1996), we fitted the coefficients of restitution of snow to describe the porosity dependence, though we used f where they used v_i, as follows:

$$\varepsilon = \varepsilon_0 f^{-k \log f}, \tag{2}$$

where ε_0 and k were fitting parameters and were obtained to be $\varepsilon_0 = 0.90 \pm 0.02$ and $k = 10.5 \pm 0.4$. However, we note that Eq. (2) was applied under very limited conditions such as the impact velocity from 0.4 to 4.4 m s^{-1} and the temperature of -10 °C. We expected that the local disruption near the impact point would drastically reduce the coefficient of restitution at the high impact velocity, but at the low impact velocity it might decrease because of adhesive force. Based on the minimum reliable value of ε for bouncing, we define ε_b as the upper limit of the threshold value separating bounce mode from no-bounce mode in this study, and ε_b was obtained to be 0.029. Moreover, when we put $\varepsilon_b = 0.029$ into

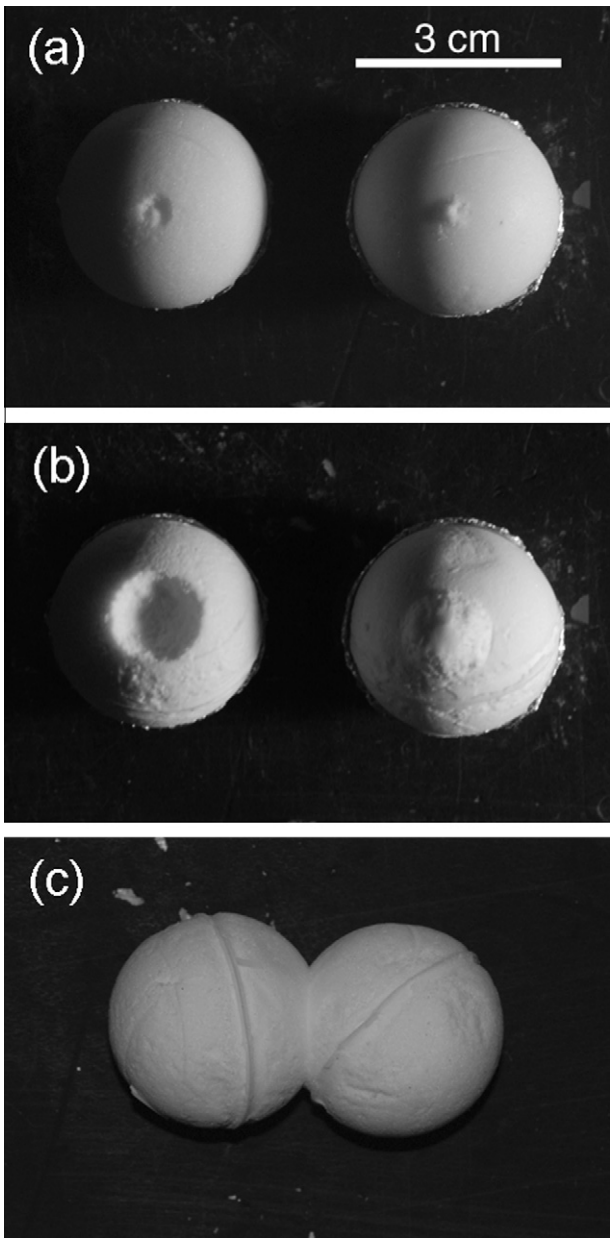

Fig. 4. The photograph of the recovered samples showing the contact area for (a) 44% porosity at 3.5 m s^{-1} and (b) 70% porosity at 3.2 m s^{-1}. Mass transfer from the target (left) to the projectile (right) can be seen. (c) The stuck dimer sample recovered from on the airbag for 80% porosity at 3.4 m s^{-1}.

Eq. (2), we derive the critical filling factor f_{crit} = 0.42 corresponding to the boundary; which means that sticking does not occur at f > 0.42.

As mentioned above, the coefficient of restitution of silicate dust aggregates decreases with the increase of the porosity, but it barely reaches 0 because of the 'bouncing barrier'. In Fig. 3c the data of silicate dust aggregates are plotted for comparison (Beitz et al., 2011; Blum and Münch, 1993; Fujii and Nakamura, 2009; Heiβelmann et al., 2007, 2010; Weidling et al., 2012). The experimental conditions of these studies are summarized in Table 2, and it was found that the silicate dust aggregates stuck together at low collision velocities. For example, the mm-sized silicate dust aggregates with f = 0.35 often stuck together at velocities lower than 0.03 m s^{-1}, but most of the results were in the bounce mode in the velocity range from 0.001 to 1 m s^{-1} (Weidling et al., 2012). On the other hand, the coefficient of restitution of snow with $f < f_{crit}$ at v_i < 5 m s^{-1} was nearly 0, corresponding to no-bounce or sticking mode. This means that our snow sample is able to coagulate at a velocity higher than that required for silicate dust aggregates.

3.2. Mass transfer

To study the mass transfer between an impactor and a target, we recovered both samples after the collision and measured these masses to check the mass loss and the mass gain, and we calculated the mass change, defined as m_{i2}/m_{i1}, where subscript i denotes the target or projectile, and 1 and 2 denote before and after the collision, respectively. We also measured the width, W, of the contact area between them, which was defined as the average width of a hollow or a projection shown in Fig. 4. Fig. 4 shows the photos of recovered samples with the porosity of (a) 44%, (b) 70% and (c) 80% impacted at the velocity of ~3 m s^{-1}. One can see that a small amount of surface material on one side has eroded and is stuck on another side. The mass transfer from the target (left) to the projectile (right) can be recognized in Fig. 4a and b. However, two types of mass transfer occurred; the mass gain was observed 11 times on the impactor and 5 times on the target. The width of the contact area and the amount of mass transfer were found to increase with the increase of the porosity and the impact velocity. According to the analysis of recorded high-speed images, we found that the impactor sometimes stuck on the target during the collision, but the two attached snowballs were usually separated by the landing shock (Fig. 4b). We found a difference in the mass change in the samples with the porosity of 70%, depending on the sintering duration; the mass change of samples sintered for 1 or 2 days was less than that of samples sintered for 15 min because of shallow crater depth. The width of the contact area was almost comparable among samples, irrespective of the sintering duration (Fig. 5). This curiosity might have been caused by the modification of the sample surface during the sintering, and the adhesion force at the sample interface might have been reduced during the sintering. Fig. 4c shows the recovered snowballs sticking to each other following the collision between 80% porosity snowballs, and we could pick up the sample without the two balls separating, which means that the adhesion force at the interface was large enough to overcome the tensile stress at the interface generated by the gravity force.

Fig. 5 shows the relationship between the mass change (m_{i2}/m_{i1}) of the projectile/target and the impact velocity. Each set of data connected by a vertical line corresponds to a pair of recovered samples in one experiment. The data from one experiment should be symmetrical with respect to the horizontal line at unity, though we sometimes experienced unavoidable mass loss by erosion and sublimation during the experiment, which caused some pairs to be offset. Although the snowballs with the porosity larger than 70% stuck to each other during impact, most of these pairs were separated by the landing shock. Only one sample with 80% porosity was recovered without separation, and it is shown by an arrow. The mass transfer of bouncing snowballs was less than 1% of the initial mass, and it happened at the porosity lower than 60%.

3.3. Collisional deformation

As shown in Fig. 4, the contact area was found to increase with increasing the porosity. Fig. 6 shows the width of the contact area normalized by a snowball diameter (W/D) as a function of the impact velocity for each porosity sample. The error bars indicate the variation of the width of the contact area caused by the irregularity of the shape deviated from a circle. The results obtained for a porous gypsum ball were also plotted for comparison. Fujii and

Table 2
List of experimental conditions for references.

Projectile				Target material	Velocity (m s^{-1})	Reference
Material	Filling factor	Shape	Diameter (mm)			
Ice	0.2–0.56	Sphere	30	Same	0.44–4.12	This study
Ice	0.4–0.6	Sphere	10	Same block	1.8–2.8	This study
Ice	1	Sphere	30	Ice block	0.01–10	Higa et al. (1996)
Ice with frost	1	Sphere	15	Same	0.06–0.22	Heiβelmann et al. (2010)
SiO_2 beads	1	Sphere	10	Same	0.003–0.05	Heiβelmann et al. (2010)
SiO_2 dust	0.15	Cube	2–5	Same	0.1–0.5	Heiβelmann et al. (2007)
SiO_2 dust	0.50	Sphere	30	Same	0.01–0.5	Beitz et al. (2011)
SiO_2 dust	0.35	Sphere	0.5–2	Same	0.001–1	Weidling et al. (2012)
$ZrSiO_4$ dust	0.26	Irregular	0.2–5	Same	0.15–4	Blum and Münch (1993)
Gypsum	0.39–0.69	Sphere	50	Steel plate	0.1–10	Fujii and Nakamura (2009)

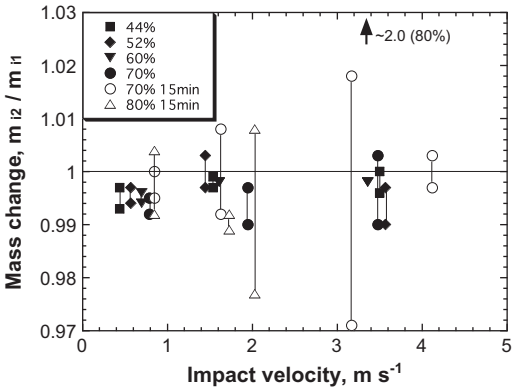

Fig. 5. The mass change of the target/projectile during impact as a function of the impact velocity. The vertical lines connecting two plots denote a target and projectile pair used in one experiment. The stuck dimer for the 80% sample is shown by an arrow at the top of the figure.

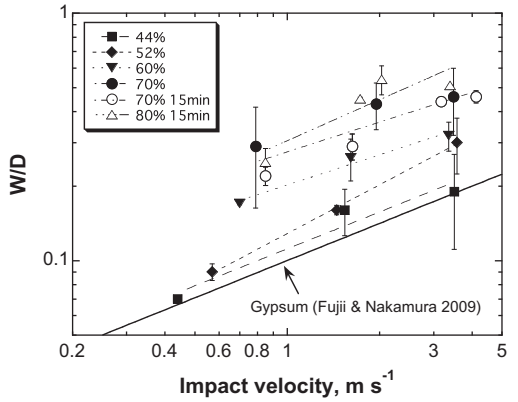

Fig. 6. The relationship between the contact area width normalized by sample diameter and the impact velocity. Error bars display the variation of the contact area width. The data of gypsum impacted on an iron plate is plotted for comparison (Fujii and Nakamura, 2009).

Nakamura (2009) used a gypsum ball with the size of 50 mm and $f = 0.39–0.69$ that was impacted on an iron plate. We found that the normalized width of the contact area increased with the increase of the impact velocity but was almost independent of the sintering duration for 70% porosity snowballs, and more snowballs had a larger normalized width compared to that obtained for porous gypsum balls. This difference between snow and porous gypsum was caused by their material strength. The compressive strength of snow is 0.01–1 MPa in this porosity range (Mellor, 1975), but that of porous gypsum is 7.6–18.7 MPa (Fujii and Nakamura, 2009). Each set of porosity data for snowballs can be fitted by the following power law equation irrespective of sintering duration:

$$W/D = pv_i^q, \tag{3}$$

where p and q are fitting parameters. The results are summarized in Table 3.

The energy required to compact the impact area and to grow the contact area is described by the dynamic yield strength of snow, Y_d, and the compaction volume, ΔV. The compaction volume can be calculated using the following equation, assuming that $\Delta V/2$ is a part of a hemisphere:

$$\Delta V/2 = (2/3)\pi r^3 - \pi h(3r^2 - h^2)/3, \tag{4}$$

where r is the radius of the sphere, h is the length from the center of the sphere to the compacted surface and h represents $h^2 = r^2 - (W/2)^2$. Note that in Eq. (4) $\Delta V/2$ denotes the compaction volume of one ball, because compaction occurs in both of the balls. The energy used for the compaction could be represented by the energy dissipation of the colliding balls during the impact, E_{dis}, and it is described as an initial kinetic energy of impacting balls, $E_i = \mu v_i^2/2$, where μ is a reduced mass defined as $\mu = m_p m_t/(m_p + m_t) \sim m_p/2$: $E_{dis} = E_i(1 - \varepsilon^2)$. Fig. 7 shows the relationship between the compaction volume and the dissipated kinetic energy. We notice that the compaction volume increases with the increase of the dissipated kinetic energy and the porosity, irrespective of the sintering duration. Each set of porosity data set including different sintering durations was fitted by the following power law equation:

$$\Delta V = V_0 E_{dis}^n, \tag{5}$$

where V_0 and n are fitting coefficients. These coefficients are listed in Table 3. The slope of Eq. (5), n, is between 0.80 and 1.32, and this result indicates that the compaction volume is simply proportional to the dissipated kinetic energy. In Section 4.1, we discuss the dynamic strength of snow by using this clear result regarding the relationship between compaction volume and energy dissipation.

4. Discussion

4.1. Dynamic compressive strength of snow

In Section 3.3 the compaction volume was found to be almost proportional to the dissipated kinetic energy. Taking into account the energy conservation during the collision, we obtained the following equation of energy balance:

$$E_{dis} = Y_d \Delta V. \tag{6}$$

Thus, the dynamic compressive strength, Y_d, can be represented by $Y_d = E_{dis}/\Delta V$. The energy dissipation by compaction associated with damping of vibration and friction among constituent particles is

Table 3
Results of fitting coefficients for Eqs. (3), (5), and (10).

Porosity (%)	p $(\mathrm{m\,s^{-1}})^{-q}$	q	V_0 $(\mathrm{m^3})^{-n}$	n	a $(\mathrm{m\,s^{-1}})^{1/4}$
44	0.11 ± 0.01	0.50 ± 0.12	$10^{-6.3\pm0.7}$	1.04 ± 0.26	0.197 ± 0.026
52	0.13 ± 0.01	0.66 ± 0.01	$10^{-5.7\pm0.2}$	1.32 ± 0.06	0.083 ± 0.019
60	0.20 ± 0.01	0.41 ± 0.07	$10^{-5.7\pm0.4}$	0.80 ± 0.16	0.019 ± 0.013
70	0.27 ± 0.02	0.40 ± 0.09	$10^{-5.0\pm0.4}$	0.82 ± 0.18	–
80	0.30 ± 0.05	0.55 ± 0.20	$10^{-3.7\pm1.1}$	1.11 ± 0.40	–

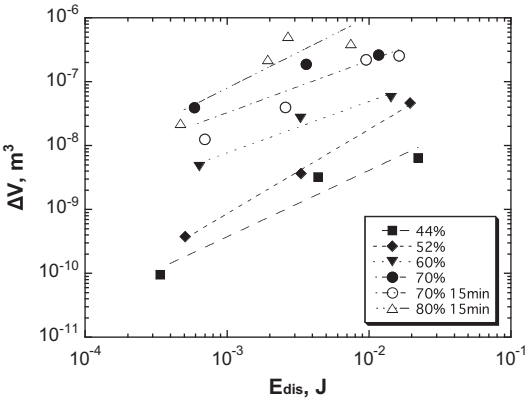

Fig. 7. The relationship between the compaction volume and the dissipated kinetic energy.

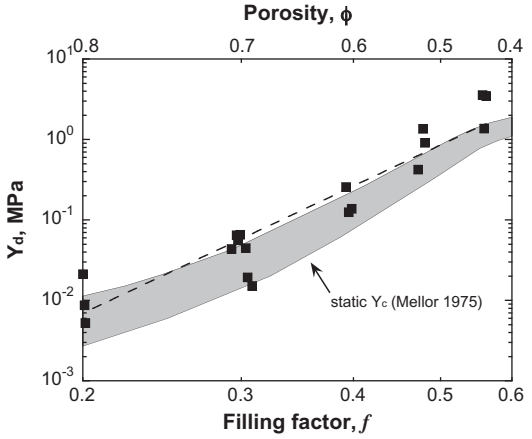

Fig. 8. The dynamic yield strength of snow as a function of the filling factor. The static compressive strength of natural snow is shown for comparison (Mellor, 1975).

assumed to be expressed in terms of $Y_d\Delta V$. Fig. 8 shows the relationship between the calculated Y_d and the filling factor for each experiment. The derived Y_d was fitted by a power law equation as follows:

$$Y_d = Y_{d0} f^l, \tag{7}$$

where $Y_{d0} = 32.6 + 22.6/-13.3$ (MPa) and $l = 5.2 \pm 0.4$. The static strength of natural snow compiled by Mellor (1975) is also shown in Fig. 8 for comparison, which was obtained under strain rates of between $10^{-4}\,\mathrm{s^{-1}}$ and $10^{-2}\,\mathrm{s^{-1}}$. We found that the dynamic compressive strength of snow is consistent with the upper limit of static compressive strength (Mellor, 1975). The strain rate in this study is estimated from the impact velocity divided by the sample length and is $\sim 10\,\mathrm{s^{-1}}$. Thus, this result indicates that the compressive strength of snow is almost independent of the strain rate up to $\sim 10\,\mathrm{s^{-1}}$.

4.2. Velocity dependence of the coefficient of restitution

In Section 3.1, we examined the velocity dependence of the coefficient of restitution and found that it hardly depended on the velocity in this experimental condition. However, it should depend on the velocity in a wide range of impact velocities, and we suspect that it increases with the decrease of the impact velocity. Therefore, we apply a theoretical model of the coefficient of restitution with plastic deformation to extrapolate our results toward lower velocity and higher velocity. Johnson (1985) developed a theoretical model of the coefficient of restitution of spherical metals at a moderate speed, and he considered an elastic–plastic deformation in the following equation:

$$\varepsilon \approx 3.8 \left(\frac{Y_d}{E^*}\right)^{\frac{1}{2}} \left(\frac{m^* v_i^2}{2 Y_d r^3}\right)^{-\frac{1}{8}}, \tag{8}$$

where $E^* = E/\{2(1-\nu^2)\}$, E and ν are Young's modulus and Poisson's ratio, respectively, $m^* = m/2$, m is the mass of a colliding body, r is the radius of a colliding body and v_i is the relative velocity at impact. The elastic moduli were calculated from the longitudinal and shear wave velocity (v_p, v_s) of the sintered snow with the porosity smaller than 60% measured by using a pulse transmitted method, written as $E = E_0 f^s$, where $E_0 = 13.4$ GPa and $s = 2.8$, and $\nu = 0.26$, respectively (Shimaki, 2010). This model assumes that the coefficient of restitution was simply controlled by the energy dissipation caused by plastic deformation of the material, and other effects such as adhesive force are neglected in his theory.

By eliminating m by using $m = (4/3)\pi\rho_i r^3 f$, where ρ_i is water ice density, and combining the elastic moduli and the porosity dependence of Y_d of Eq. (7) with Eq. (8), we obtained the following equation:

$$\varepsilon = A \cdot f^{\frac{5l-4s-1}{8}} \cdot v_i^{-\frac{1}{4}}, \tag{9}$$

where A is a constant. Eq. (9) clearly shows the velocity dependence of ε with the power law index of $-1/4$. Based on this model, the ε of snow with the porosity of 44%, 52% and 60% was fitted by the following equation:

$$\varepsilon = a v_i^{-1/4}, \tag{10}$$

where a is a fitting parameter corresponding to the elastic and plastic properties of each snowball with different porosity, as summarized in Table 3. Fig. 9 shows the fitting curves from 44% to 60% porosity as solid lines, and we can recognize weak dependence on velocity for the coefficient of restitution. To evaluate the porosity dependence on the coefficient a, we derive the power law relationship between a and f, as follows:

$$a = a_0 f^b, \tag{11}$$

where $a_0 = 11.7$ and $b = 6.9$ (Fig. 10). Then, we can interpolate and extrapolate Eq. (10) in terms of the porosity by using Eq. (11). The dotted curve in Fig. 9 shows the calculated result for 70% porosity and is found to lie on or near $\varepsilon = 0$ in this velocity range, which is consistent with our experimental result. However, when we use Eq. (8) and elastic properties of snow measured by our previous study (Shimaki, 2010), the calculated result for the 44% porosity

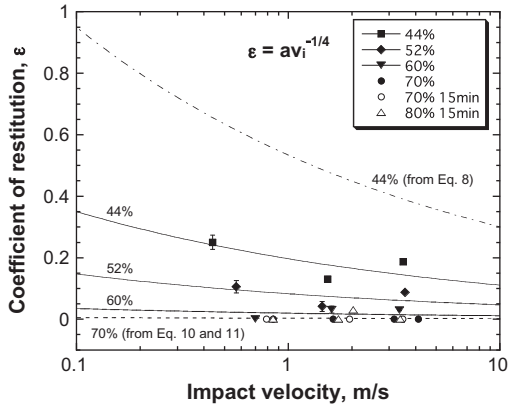

Fig. 9. Relationship between the coefficient of restitution and the impact velocity. Solid fitting curves are defined as Eq. (10). The dashed curve is a calculated result of combining Eqs. (10) and (11) for the 70% porosity sample. The dot–dash curve is a calculated result of combining Eq. (8) and elastic properties of snow obtained by Shimaki (2010).

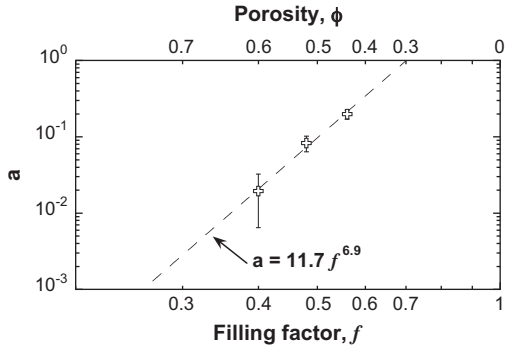

Fig. 10. Relationship between the filling factor and a in Eq. (10). The dashed curve denotes fitting by Eq. (11).

shown in Fig. 9 as a dot–dash line is found to disagree with our experimental results. This suggests that additional effects that are neglected in Eq. (8) such as adhesive force might reduce the coefficient of restitution of snow (e.g., Thornton and Ning, 1998). However, it is difficult to estimate the adhesive force of snow from this experimental result because of lack of low-velocity data smaller than 0.1 m s^{-1}. By combining Eqs. (10) and (11), we obtain the relationship between f and v_i, as follows:

$$f = (\varepsilon/a_0)^{1/b} v_i^{1/4b}, \tag{12}$$

and this equation can describe the contour map of the coefficient of restitution in terms of f and v_i.

Fig. 11 shows collisional outcomes of equal-sized snowballs as a function of filling factor and impact velocity. Using Eq. (12), we plotted the contours of the coefficient of restitution for $\varepsilon = 0.3$, 0.03 and 0.003, as shown in Fig. 11. The boundary between bounce and no-bounce or sticking is almost consistent with the contour for $\varepsilon = 0.03$ and is shown by a bold solid curve; it is written as $f = 0.42 \times v_i^{0.036}$. The parameter $\varepsilon = 0.03$ can explain the upper limit of the experimental condition corresponding to no-bounce or sticking and well classify the collisional outcomes. At the impact velocity larger than 10 m s^{-1}, the disruption should occur as reported in our previous study (Shimaki and Arakawa, 2012). The dashed and dotted curves in Fig. 11 denote the shattering strength (Q^*) of snow, defined as the impact energy per unit mass (= energy density) when the largest fragment mass equals half of the original target mass; for the porosity larger than 40%, $Q^* = 200 \times f^{1.5}$

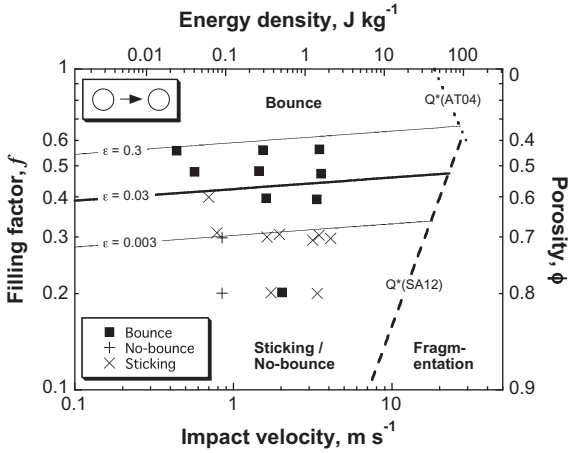

Fig. 11. Diagram for collisional outcomes for equal-sized snowballs at the impact condition described by the impact velocity and the filling factor. The solid curves are calculation results of Eq. (12) using $\varepsilon = 0.3$, 0.03 and 0.003, respectively. The $\varepsilon = 0.03$ of the bold solid curve can explain the upper limit of the sticking/no-bounce mode. The dashed and dotted curves are Q^* of snow for $\phi > 0.4$ (Shimaki and Arakawa, 2012) and for $\phi < 0.4$ (Arakawa and Tomizuka, 2004) under the assumption that Q^* does not depend on the mass ratio.

(Shimaki and Arakawa, 2012), and for the porosity smaller than 40%, $Q^* = 42.8 \times f^{-1.8}$ (Arakawa and Tomizuka, 2004). In the previous studies the mass ratio of projectile to target (m_p/m_t) was limited to be smaller than 0.05, so we assumed that Q^* did not depend on the mass ratio and applied Q^* in Fig. 11 with consideration of the energy density, which was calculated to be $Q = E_i/(m_p + m_t) = v_i^2/8$ for equal-mass collision. The boundary conditions of fragmentation are as follows: $f = 0.0073 \times v_i^{1.3}$ for the porosity larger than 40% and $f = 25.7 \times v_i^{-1.1}$ for the porosity smaller the 40%. The dashed and dotted curves could be the maximum velocity for the boundary between fragmentation and bounce or no-bounce/sticking, because fragmentation usually begins at Q that is slightly smaller than Q^*. To understand collisional disruption of equal-sized bodies in the higher velocity region, additional experiments would be necessary at $v_i > 5$ m s^{-1}.

Fig. 11 shows the interesting feature that equal-sized snowballs with $f < 0.4$ can stick to each other at the impact velocity up to 5 m s^{-1}, and thus we speculate that this might enable ice aggregates in the solar nebula to grow continuously by direct impact sticking, even among centimeter-sized aggregates at the filling factor f smaller than 0.4. Additionally, different-sized collisions would encourage further growth, because in that case the boundary condition of fragmentation would move to a higher velocity.

Fig. 11 is derived for the snow sample made of 30-μm ice aggregates sintered at −10 °C in air, so this sintering condition was far from that in the outer Solar System: the temperature was below 100 K in vacuum. Therefore, it is difficult to apply our results to snow collisions in the outer Solar System. However, this figure might be applicable with regard to the collisional outcome around the snow line in the solar nebula. The temperature of the snow line in the solar nebula is estimated to be ~160 K at the heliocentric distance of ~3 AU for the minimum mass solar nebula model (Hayashi et al., 1985; Sirono, 2011). At that temperature, ice aggregates composed of small particles with the radius of 0.1 μm were quickly sintered, and the mean particle size of ice grains grew to 10 μm within 10 years (Kuroiwa and Sirono, 2011). Thus, the particle size in our study fortunately simulates the ice particle size in the case of staying near the snow line more than 10 years in the solar nebula. The sintering process among ice particles makes ice aggregate more elastic (Sirono, 1999), and thus our sintered snow sample could bounce in collisions rather than sticking, which gave us the

idea that the ice aggregates near the snow line could also bounce in accordance with Fig. 11.

In addition to the continuous sintering process, our experimental temperature of −10 °C (263 K) might be serious for the effects of instantaneous sintering and adhesion enhanced by a quasi-liquid layer on an ice surface. The necks among ice particles grow up to 1 μm within 1 ms by sintering at 263 K (Kuroiwa and Sirono, 2011), and that instantaneous duration is comparable to the contact duration between snowballs observed in our collision experiment. However, such a thin neck less than 1 μm would not have sufficient cohesion force at the interface of colliding snowballs to stick them to each other. The thickness of a quasi-liquid layer at 263 K was reported to be from 0.1 to 40 nm, depending on the measurement method (Petrenko and Whitworth, 1998), which shows that the layer is much thinner than the particle diameter of 21 μm. It might be difficult for the thin layer to enhance the adhesion between snowballs. Therefore, we speculate that the effects of instantaneous sintering and adhesion by a quasi-liquid layer are not so important with regard to the sticking among snowballs during the contact. Further investigation and immediate confirmation of the temperature dependence of sticking among snowballs are strongly desired. However, other physical effects on sticking caused by collision such as impact melting and air-cushioning are negligible, because the impact velocity is very low as small as 1 m s^{-1} and the deformed contact area is very small.

We conclude that our experimental result shown in Fig. 11 indicates the porosity and velocity dependencies of collisional outcomes for the sintered ice aggregates in the solar nebula, which would exist near the snow line. However, since Fig. 11 was obtained from a head-on collision and a laboratory environment, further experimental and theoretical studies are necessary to conduct these experiments at low temperatures suitable for the outer Solar System or the solar nebula in vacuum.

Acknowledgments

We appreciate Dr. S.J. Weidenschilling and an anonymous referee for their helpful review on our manuscript. We are grateful to S. Nakatsubo of the Contribution Division of the Institute of Low Temperature Science, Hokkaido University, for his technical help. We acknowledge the hospitality of the Center for Planetary Science (CPS) for providing a place for working. This work was supported by a grant-in-aid for scientific research (10J07305, 20340118, 23103004) from the Japan Ministry of Education, Culture, Sports, Science and Technology, and a grant from the Joint Research Program of the Institute of Low Temperature Science, Hokkaido University.

Appendix A. Supplementary material

Supplementary data associated with this article can be found, in the online version, at http://dx.doi.org/10.1016/j.icarus.2012.08.005.

References

Arakawa, M., Tomizuka, D., 2004. Ice–silicate fractionation among icy bodies due to the difference of impact strength between ice and ice–silicate mixture. Icarus 170, 193–201.

Beitz, E., Güttler, C., Blum, J., Meisner, T., Teiser, J., Wurm, G., 2011. Low-velocity collisions of centimeter-sized dust aggregates. Astrophys. J. 736, 34. http://dx.doi.org/10.1088/0004-637X/736/1/34.

Blum, J., 2010. Dust growth in protoplanetary disks – A comprehensive experimental/theoretical approach. Res. Astron. Astrophys. 10, 1199–1214.

Blum, J., Münch, M., 1993. Experimental investigations on aggregate–aggregate collisions in the early solar nebula. Icarus 106, 151–167.

Blum, J. et al., 2000. Growth and form of planetary seedlings: Results from a microgravity aggregation experiment. Phys. Rev. Lett. 85, 2426–2429.

Bridges, F.G., Hatzes, A.P., Lin, D.N.C., 1984. Structure, stability and evolution of Saturn's rings. Nature 309, 333–335.

Cuzzi, J. et al., 2009. Ring particle composition and size distribution. In: Dougherty, M., Esposito, L., Krimigis, T. (Eds.), Saturn from Cassini-Huygens. Springer, New York, pp. 459–509.

Fujii, Y., Nakamura, A.M., 2009. Compaction and fragmentation of porous gypsum targets from low-velocity impacts. Icarus 201, 795–801.

Goldreich, P., Ward, W.R., 1973. The formation of planetesimals. Astrophys. J. 183, 1051–1062.

Güttler, C., Blum, J., Zsom, A., Ormel, C.W., Dullemond, C.P., 2010. The outcome of protoplanetary dust growth: Pebbles, boulders, or planetesimals? I. Mapping the zoo of laboratory collision experiments. Astron. Astrophys. 513, A56. http://dx.doi.org/10.1051/0004-6361/200912852.

Hatzes, A.P., Bridges, F.G., Lin, D.N.C., 1988. Collisional properties of ice spheres at low impact velocities. Mon. Not. R. Astron. Soc. 231, 1091–1115.

Hayashi, C., Nakazawa, K., Nakagawa, Y., 1985. In: Black, D.C., Matthews, M.S. (Eds.), Protostars and Planets II. Univ. of Arizona Press, Tucson, AZ, p. 1100.

Heiβelmann, D., Fraser, H.J., Blum, J., 2007. Experimental studies on the aggregation properties of ice and dust in planet-forming regions. In: Proc. 58th Int. Astron. Congress 2007.

Heiβelmann, D., Blum, J., Fraser, H.J., Wolling, K., 2010. Microgravity experiments on the collisional behavior of saturnian ring particles. Icarus 206, 424–430.

Higa, M., Arakawa, M., Maeno, N., 1996. Measurements of restitution coefficients of ice at low temperatures. Planet. Space Sci. 44, 917–925.

Higa, M., Arakawa, M., Maeno, N., 1998. Size dependence of restitution coefficients of ice in relation to collision strength. Icarus 133, 310–320.

Johnson, K.L., 1985. Contact Mechanics. Cambridge University Press, Cambridge.

Kuroiwa, T., Sirono, S., 2011. Evolution of distribution of icy grains by sublimation and condensation. Astrophys. J. 739, 18. http://dx.doi.org/10.1088/0004-637X/739/1/18.

Mellor, M., 1975. A Review of Basic Snow Mechanics. IAHA-AISH Publ. 114, p. 251.

Okuzumi, S., Tanaka, H., Sakagami, M., 2009. Numerical modeling of the coagulation and porosity evolution of dust aggregates. Astrophys. J. 707, 1274. http://dx.doi.org/10.1088/0004-637X/707/2/1247.

Petrenko, V.F., Whitworth, R.W., 1998. Physics of Ice. Oxford University Press, New York.

Schmidt, J., Ohtsuki, K., Rappaport, N., Salo, H., Spahn, F., 2009. Dynamics of Saturn's dense rings. In: Dougherty, M., Esposito, L., Krimigis, T. (Eds.), Saturn from Cassini-Huygens. Springer, New York, pp. 413–458.

Shimaki, Y., 2010. Experimental Study on the Collisional Accretion Process of Icy Planetesimals in Thermal Evolution. M.S. Thesis, Nagoya University, Japan.

Shimaki, Y., Arakawa, M., 2012. Experimental study on collisional disruption of highly porous icy bodies. Icarus 218, 737. http://dx.doi.org/10.1016/j.icarus.2012.01.021.

Sirono, S., 1999. Effects by sintering on the energy dissipation efficiency in collisions of grain aggregates. Astron. Astrophys. 347, 720–723.

Sirono, S., 2011. The sintering region of icy dust aggregates in a protoplanetary nebula. Astrophys. J. 735, 131. http://dx.doi.org/10.1088/0004-637X/735/2/131.

Suyama, T., Wada, K., Tanaka, H., 2008. Numerical simulation of density evolution of dust aggregates in protoplanetary disks. I. Head-on collisions. Astrophys. J. 684, 1310–1322.

Thornton, C., Ning, Z., 1998. A theoretical model for the stick/bounce behaviour of adhesive, elastic–plastic spheres. Powder Technol. 99, 154–162.

Wada, K., Tanaka, H., Suyama, T., Kimura, H., Yamamoto, T., 2007. Numerical simulation of dust aggregate collisions. I. Compression and disruption of two-dimensional aggregates. Astrophys. J. 661, 320–333.

Wada, K., Tanaka, H., Suyama, T., Kimura, H., Yamamoto, T., 2008. Numerical simulation of dust aggregate collisions. II. Compression and disruption of three-dimensional aggregates in head-on collisions. Astrophys. J. 677, 1296–1308.

Wada, K., Tanaka, H., Suyama, T., Kimura, H., Yamamoto, T., 2009. Collisional growth conditions for dust aggregates. Astrophys. J. 702, 1490. http://dx.doi.org/10.1088/0004-637X/702/2/1490.

Wada, K., Tanaka, H., Suyama, T., Kimura, H., Yamamoto, T., 2011. The rebound condition of dust aggregates revealed by numerical simulation of their collisions. Astrophys. J. 737, 36. http://dx.doi.org/10.1088/0004-637X/737/1/36.

Weidenschilling, S.J., 1977. Aerodynamics of solid bodies in the solar nebula. Mon. Not. R. Astron. Soc. 180, 57–70.

Weidenschilling, S.J., Cuzzi, J.N., 1993. In: Levy, E.H., Lunine, J.I. (Eds.), Protostars and Planets III. Univ. of Arizona Press, Tucson, AZ, p. 1031.

Weidling, R., Güttler, C., Blum, J., Brauer, F., 2009. The physics of protoplanetesimal dust agglomerates. III. Compaction in multiple collisions. Astrophys. J. 696, 2036. http://dx.doi.org/10.1088/0004-637X/696/2/2036.

Weidling, R., Güttler, C., Blum, J., 2012. Free collisions in a microgravity many-particle experiment. I. Dust aggregate sticking at low velocities. Icarus 218, 688. http://dx.doi.org/10.1016/j.icarus.2011.10.002.

Zsom, A., Ormel, C.W., Güttler, C., Blum, J., Dullemond, C.P., 2010. The outcome of protoplanetary dust growth: Pebbles, boulders, or planetesimals? II. Introducing the bouncing barrier. Astron. Astrophys. 513 (2010), A57. http://dx.doi.org/10.1051/0004-6361/200912976.